A MEMS device for *In Situ* TEM/AFM/SEM/STM Testing of Carbon Nanotubes and Nanowires

H. D. Espinosa, Y. Zhu and B. Peng
Department of Mechanical Engineering, Northwestern University
2145 Sheridan Road, Evanston, IL 60208-3111, USA

ABSTRACT
A MEMS device for *in-situ* TEM/AFM/SEM/STM testing of nano structures is designed. Two deformation measurement methods are discussed: microscopic measurement and electrical measurement. For the first method, the device consists of a comb-drive actuator, calibration beam and specimen stage. The stiffness of the specimen can be well characterized by comparing the load-displacement relation before and after the attachment of the specimen. For the second method, the device is composed of a comb-drive actuator, specimen stage and a beam-type load sensor. The load and displacement of the specimen are measured independently. Deformation fields will be obtained by means of a full field technique, with natural or artificial nano patterns to be correlated, while the load sensor identifies the load applied to the specimen by measuring voltage changes. This device demonstrates the feasibility of ultra-high resolution mechanical property measurements in small systems by means of MEMS techniques. The subsequent experiments are expected to identify the mechanical properties such as fracture, fatigue, and inelastic deformation mechanisms of nano structures, by quantifying defect sources, their kinetics, and interactions.

INTRODUCTION
The Young's modulus, strength and toughness of nanostructures (carbon nanotubes, nanowires) are important to proposed applications ranging from nanocomposites to probe microscopy and nanoelectronics, yet there is little direct knowledge of these key electromechanical properties. After the discovery of carbon nanotubes [1, 2, 3], they were predicted theoretically to possess structural perfection, high stiffness and high strength. There have been a lot of experimental studies on the mechanical properties of nanotubes. Treacy, et al. [4] measured the amplitude of intrinsic thermal vibration of nanotubes inside the transmission electron microscope (TEM); Wong, et al. [5] bent nanotubes with an AFM operated in lateral force mode; Poncharal, et al. [6] electrically drove the cantilevered nanotubes at resonance inside TEM; Yu, et al. [7] stretched nanotubes with a “nanostressing stage” under SEM; and Salvetat et al. [8] applied AFM to deflect the nanotubes over the patterned holes.

However, all these methods are indirect, based on various assumptions and limited accuracy. To date there is no direct tension or compression testing on nanotubes yet, due to the difficulties in manipulating the nanotubes and precisely measuring the displacements and corresponding loads. In this paper, two measurement mechanisms based on MEMS technology render the feasibility of direct tension or compression testing of carbon nanotubes.

MEMS TESTING METHODOLOGY
For the mechanical testing of Carbon Nanotubes (CNTs) and nanowires, there are basically two techniques schematically shown in Figure 1. In (a), after a long slender beam is buckled, the displacement of the specimen is measured by recording the lateral deflection of the buckling beam [9]. In (b), the displacement is measured by microscopy, and the corresponding load by a capacitive sensing based load sensor.

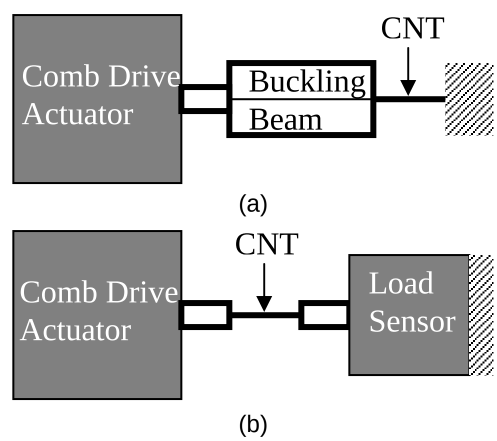

Fig. 1. (a) CNT testing with buckling beam to measure both deformation and force of CNT. The left portion is a comb drive actuator, the central portion is a frame enclosing a long slender beam, and the right portion is the sample. (b) CNT testing with load sensor to measure the force of CNT, while the deformation is observed by atomic probe microscopy. The left portion is a comb drive actuator, central portion is the sample, and the right portion is load sensor.

BUCKLING BEAM BASED METHOD
As shown in Figure 1 (a), the device consists of a comb drive actuator, a buckling beam based sensor and the specimen. The force generated by the comb drive actuator is given by [9]

$$F = N\varepsilon_0 \frac{h}{d} V^2 = \beta V^2 \qquad (1)$$

Proceedings of the 2002 SEM Annual Conference & Exposition on Experimental and Applied Mechanics, June 10-12, Milwaukee, Wisconsin, Session 18, Paper 110, 2002.

where

N	number of moving and fixed comb pairs;
ε_0	permittivity constant;
h	height of the combs;
d	lateral gap between the fixed and moving combs.
V	actuation voltage

These constants can be expressed as a unified constant β. A long slender beam subjected to an axial compressive force buckles when the force exceeds a critical value of

$$P_{cr} = H\pi^2 EI / L^2 \qquad (2)$$

where the constant *H* depends on the boundary conditions, e.g. *H* = 4 for beams of double ends clamped, which is applicable to the current setup. *E* is the Young's modulus, *I* is the minimum moment of inertia equal to $b^3h/12$ with width *b* and height *h*, and *L* is the length of the beam. P_{cr} is calculated based on measured beam dimensions and knowledge of the material of the beam.

The actuator generates a compressive force on the beam and buckles it at the critical value, which can be used to find the value of β as seen in following equation.

$$\beta V_0^2 = P_{cr} \qquad (3)$$

With increased actuation force, the buckled beam continues to be deformed with an axial displacement of δ. A first order approximation of the force balance is given by

$$\beta V_1^2 = k_1\delta + P_{cr}(1+\frac{\delta}{2L}) \qquad (4)$$

where

V_1	applied voltage;
β	calibration parameter defined in (1);
k_1	spring constant of the actuator;
L	length of the calibration beam.

The spring constant of the actuator is measured when the axial displacement is recorded. The axial displacement is usually tiny, however the lateral displacement (*D*) of the calibration beam is much larger. The lateral displacement is measured with vernier scales, which has a 50 nm resolution in an optical measurement. A nanometer resolution can be obtained if the experiment is conducted under an SEM. The relation between D and δ is given by

$$\delta = \frac{\pi^2 D^2}{4L} \qquad (5)$$

For a given 500 μm long beam, when δ = 0.01 μm, *D* = 1.424 μm (142 times amplification); when δ = 0.1 μm, *D* = 4.5 μm (45 times amplification). By this means, the axial displacement can be measured within nanometer resolution.

After the device is returned to the unactuated state, the CNT is suspended, over the anchor and comb drive attachment, using a nanomanipulator [10]. By increasing the voltage, the calibration beam should buckle at the same voltage as before. When the voltage continues to increase, at the same displacement, the voltage is different from the previous case without CNT. The force balance is changed to

$$\beta V_2^2 = k_2\delta + P_{cr}(1+\frac{\delta}{2L}) \qquad (6)$$

Here k_2 is the sum of the actuator spring constant and the specimen spring constant. By comparing k_1 and k_2, the spring constant of specimen can be determined if the spring constant of the actuator is well characterized. An assumption is that both specimen and actuator have the same axial displacement, which is reliable since the spring constants of specimen and actuator are far less than that of the interconnection. Integrating equations (3), (4) and (6), a simple relation between the spring constant and comb drive actuation voltage is expressed as follows and shown in Figure 2 as well.

$$\beta(V_2^2 - V_1^2) = (k_2 - k_1)\delta \qquad (7)$$

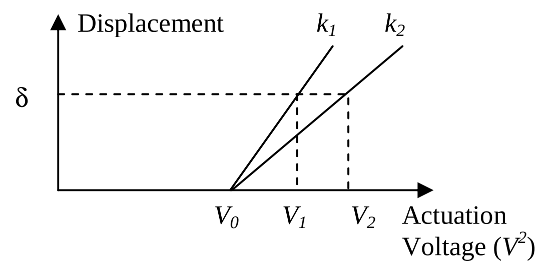

Fig. 2. The different actuation voltages at the same displacement with and without specimen.

Two calibration approaches of the actuator spring constant are discussed in following. The first method is based on the dimensions of support beams, which can be well measured under microscopy with high resolution [11]. Polysilicon shows various crystalline structures under different deposition conditions, such that the mechanical properties vary significantly. A specific polysilicon membrane deposited on top of SiO_2, on the same chip, can be used for membrane deflection experiment (MDE) [12, 13, 14] to identify the Young's modulus. The spring constant is then calculated with beam theory. The second method is to resonate the comb drive actuator. An identical comb drive with calibration beam will be fabricated on the same chip and driven at resonance. The equation between spring constant and resonant frequency is given by

$$f_r = \frac{1}{2\pi}[\frac{k_1}{(M_P + 0.3714M)}]^{1/2} \qquad (8)$$

where M_P and M are the masses of the plate and of the supporting beams, respectively.

CAPACITIVE SENSING BASED METHOD

In this approach, the load sensor is based on differential capacitive sensing as shown in Figure 3. The movement of the movable electrode is equal to the deformation of the folded beams in axial direction. Capacitance change is approximately proportional to the movement of movable electrode. If a voltage bias V_0 is applied on each fixed electrode there will be a voltage change in the moving electrode, V_{sense}, given as:

$$\frac{V_{sense}}{V_0} = \frac{\Delta d}{d} + o\left(\frac{\Delta d}{d}\right)^3 \qquad (9)$$

where d is the gap between movable and fixed electrodes , Δd the movable electrode displacement in the axial direction, and V_0 the bias voltage (about 10 V). If the spring constant of the folded beams is characterized, the force applied on the load cell is proportional to V_{sense}. The displacement of the nanotube is comparatively very small (within 100 nm, about 5% of the gap); hence, parallel plate differential capacitive sensor offers the desired resolution.

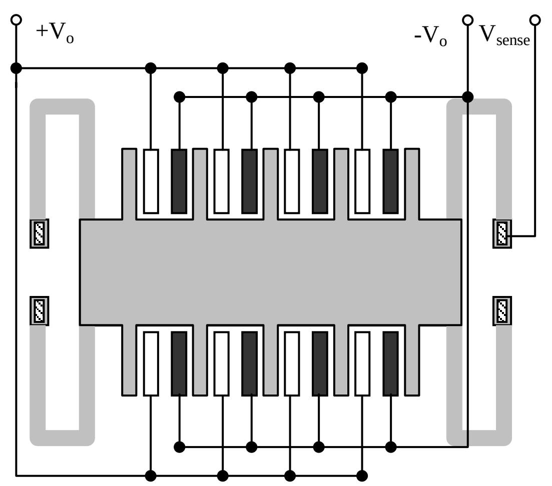

Fig. 3. A schematic of differential capacitive sensor.

However, due to the existence of parasitic capacitance, equation (9) is not practically true. Equation (10) considers parasitic capacitance.

$$\frac{V_{sense}}{V_0} = \frac{C_1 - C_2}{C_1 + C_2 + C_p} \qquad (10)$$

where C_1 is the capacitance before deflection, C_2 the capacitance after deflection and C_p the parasitic capacitance. The parasitic capacitance reduces the signal significantly.

One way to mitigate this problem is to integrate the CMOS circuitry with the mechanical sensor. However, this does add much fabrication complexity. The alternative is to design elaborate measurement circuit in open-loop or closed-loop. Figure 4 shows an open-loop circuit which is able to effectively eliminate the parasitic capacitance. The disadvantage is that for small value it would require an extremely low amplifier input capacitance for accurate open-loop sensing, but with closed-loop operation the error contribution due to variations in gain is negligible if the demodulator gain is high, as shown in Figure 5.

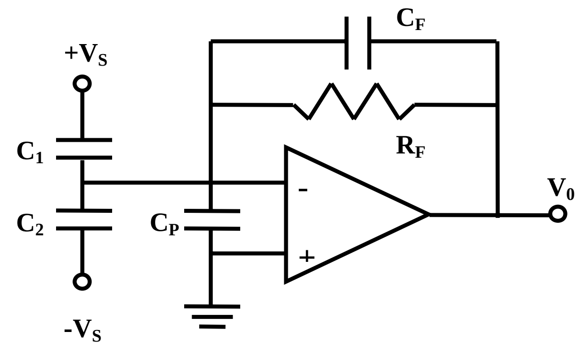

Fig. 4. Open-loop circuit to eliminate parasitic capacitance. [15]

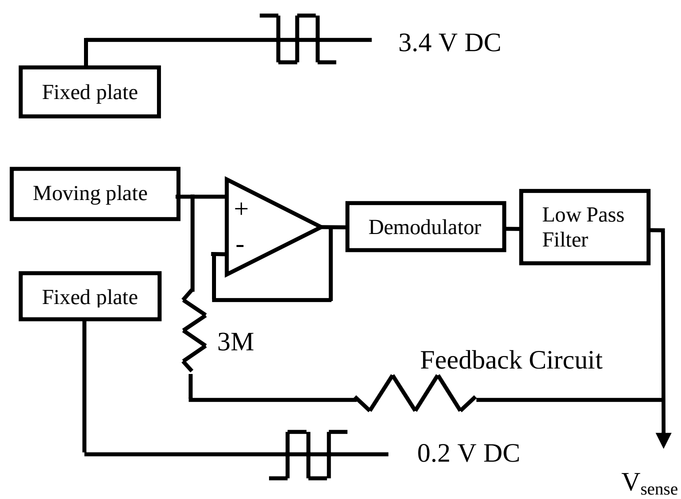

Fig. 5. Closed-loop operation coupled with high amplifier gain can be used to handle small capacitance change, similar to Analog Devices' capacitive accelerometer. [16]

CALIBRATION OF CAPACITIVE SENSING

Though the above circuits illustrate a way to measure the displacement, calibration must be done to verify the results. Several calibration methods are discussed as follows.

a). Buckling Beam Calibration

After beam buckling, various actuation voltages result in axial displacements (δ) of the load sensor, which are amplified as lateral displacements (D) measured by the vernier. At the same time, corresponding voltages applied to the load sensor are recorded and an electron microscope is used to measure load frame deflections. A calibrated relation of sensed voltages and axial displacements is drawn, which can be used as criteria for subsequent tests.

b). Laser Interferometric Calibration

A laser interferometer, with active feedback control, is employed to measure displacements with picometer resolution. Sinusoidal or pulse signals are applied to the comb drive actuator. The displacement is measured by the interferometer and voltage change is recorded by a computer through ADC.

c). Vernier Calibration
A vernier parallel to the actuator motion is fabricated close to the capacitive sensor. A field emission SEM with the resolution of 1 nm is used in conjunction with this vernier.

d). Atomic Force Microscope (AFM) Calibration
In this calibration methodology, an AFM tip is hooked to the load sensor and laterally deforms it, while the voltage change is recorded electronically. The lateral motion of the AFM can be controlled with a resolution of 1 nm.

DEVICE FABRICATION PROCESS

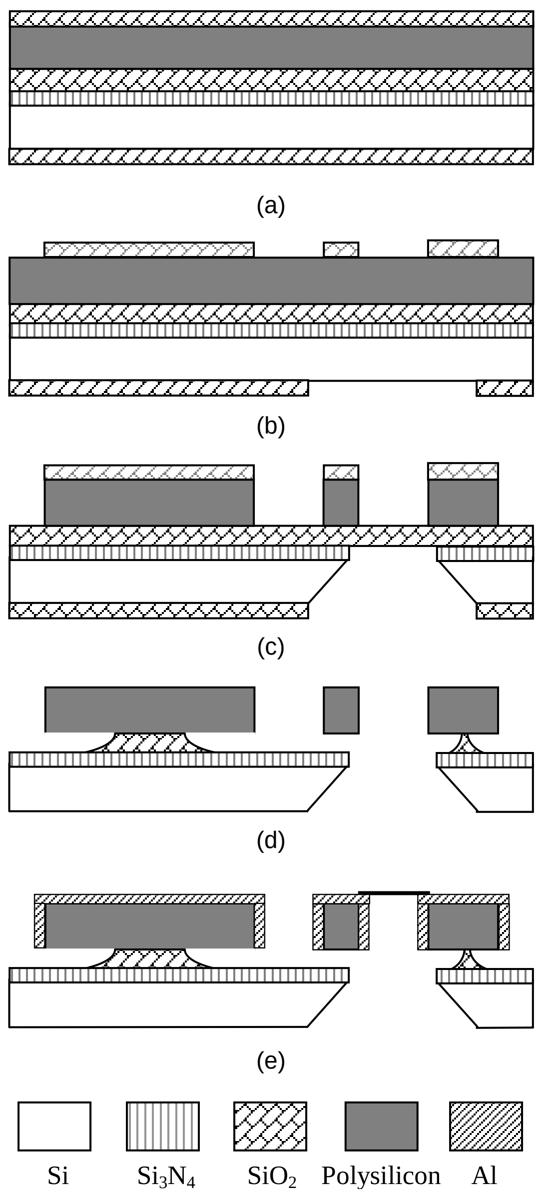

Fig. 6. The fabrication process of the MEMS testing device.

The fabrication process is illustrated in Figure 6 and summarized as follows. 0.5 μm Si_3N_4 is deposited on top of a (100) silicon wafer. 2 μm oxide is deposited serving as a sacrificial layer. 4 μm polysilicon is deposited by Low Pressure Chemical Vapor Deposition (LPCVD) at 580°C using SiH_4 gas. The as-deposited film is at least partially amorphous, and is annealed at 1100°C, during which treatment, crystallization to a fine-grained polycrystalline microstructure occurs. 0.5 μm SiO_2 is then deposited by LPCVD at 450°C using SiH_4 and O_2 gases for use as a masking oxide on both sides (a). Photolithography is used to pattern both sides and the masking oxide is dry etched in a CHF_3/C_2F_6 plasma (b). KOH is used to etch through the silicon wafer from backside, followed by dry etching of Si_3N_4 in Freon 14. The polysilicon is etched in Cl_2 plasma (c). Subsequently, the devices are released by immersion in aqueous hydrofluoric acid (HF) to dissolve some of the SiO_2 for a specific time, such that some oxide remains beneath the anchor pads leaving them attached to the substrate, while the movable portions are fully released. Following HF release, the devices are placed in a 25% NH_4F solution before rinsing, to help prevent stiction of the moving parts to the substrate (d). A thin layer of aluminum (0.3 μm) is then sputtered and the specimen is positioned over the bridge by a nano-manipulator under TEM (e).

CONCLUSIONS
A MEMS device has been presented for the in-situ microscopy testing of Carbon Nanotubes and Nanowires. Two variations of the device are examined. The first involves the methodology developed by Saif and co-works in which a buckling beam is used as displacement amplifier. This technique can provide accurate measurements of axial deformation of nanostructures. The second arrangement employing a differential parallel plate capacitor is proposed for measuring applied load history. Open- and closed-loop electronics can be used depending on the degree of desired linearity. In this arrangement, the nanostructure atomic deformation is independently measured by STM or conductive AFM. Using the appropriate environment, imaging of atomic structure at various deformations stages is achievable. The experiment discussed in this paper is expected to provide the needed accuracy in the measurement of electromechanical properties of Carbon Nanotubes and Nanowires.

ACKNOWLEDGMENTS
This work was sponsored by the National Science Foundation under Career Award No. CMS-9624364, by Raytheon Company through Award No. 0970-350-N711, and the Office of Naval Research YIP through Award No. N00014-97-1-0550. Work was also supported in part by the Nanoscale Science and Engineering Initiative of the National Science Foundation under NSF Award Number EEC-0118025. Special thanks are due to Prof. M. T. A. Saif of University of Illinois and Dr. H. Kahn of Case Western Reserve University for helpful discussions.

REFERENCES

1. Iijima, S., Helical microtubules of graphitic carbon, Nature, Vol. 354, pp. 56-58, 1991.
2. Iijima, S. & Ichihashi, T., Single shell carbon nanotubes of one nanometer diameter, Nature Vol. 363, pp. 603-605, 1993.
3. Bethune, D. S., Kiang, C. H., de Vires, M. S., Gorman, G., Savoy, R., Vazquez, J. & Beyers, R., Cobalt-Catalyzed Growth of Carbon Nanotubes with Single-Atomic-Layer Walls, Nature, Vol. 363, pp. 605-607, 1993.
4. Treacy, M. M. J., Ebbesen, T. W. & Gibson, J. M., Exceptionally High Young's Modulus Observed For Individual Carbon Nanotubes, Nature, Vol. 381, pp. 678-680, 1996.
5. Wong, E. W., Sheedan, P. E. & Lieber, C. M., Nanobeam Mechanics: Elasticity, Strength, and Toughness of Nanorods and Nanotubes, Science Vol. 277, pp. 1971-1975, 1997.
6. Poncharal, P., Wang, Z. L., Ugarte, D., De Heer, W. A., Electrostatic Deflections and Electromechanical Resonances of Carbon Nanotubes, Science, Vol. 283, pp. 1513-1516, 1999.
7. Yu, M. F., Lourie, O., Dyer, M. J., Moloni, K., Kelly, T. F., Ruoff, R. S., Strength and Breaking Mechanism of Multiwalled Carbon Nanotubes Under Tensile Load, Science, Vol. 287, pp. 637-640, 2000.
8. Salvetat, J. P., et al, Elastic and Shear Moduli of Single-Walled Carbon Nanotube Ropes, Phy. Rev. Let., Vol. 82, no. 5, pp. 944-947, 1999.
9. Haque, M. A. & Saif, M. T. A., Microscale Materials Testing Using MEMS Actuators, J. MEMS, Vol. 10, no. 1, pp. 146-152, 2001.
10. Lin, X., Nanoprocessing and Nanomeasurements of Carbon Nanotubes, PhD Thesis, Materials Science & Engineering, Northwestern University, 2000.
11. Saif, M. T. A. & MacDonald, N. C., Measurement of Forces and Spring Constants of Microinstruments, Rev. Scientific Instruments, Vol. 69, no. 3, pp. 1410-1421, 1998.
12. Espinosa, H. D., Prorok, B. C., and Fisher, M., Elasticity, plasticity, and fracture of thin films and MEMS materials –part I: a novel chip level testing methodology, submitted to J. Mech. Phys. Solids, 2001.
13. Espinosa, H. D., Prorok, B. C., and Fisher, M.,, A novel experimental technique for testing thin films and MEMS materials, Proc. Of the SEM Ann. Conf. On Exp. And Appl. Mech., June 4-6, 2001, Portland, Oregon, 446-449, 2001.
14. Espinosa, H. D., Zhu, Y., Fischer, M., and Hutchinson, J., An Experimental/Computational Approach to Identify Moduli and Residual Stress in MEMS RF-Switches, submitted to J. MEMS, 2001.
15. Senturia, S. D., Microsystem Design, Kluwer Academic Publishers, 2000.
16. Baxter, L. K., Capacitive Sensors: Design and Applications, IEEE press, New York, NY, 1997.